ISSN 2347-3487
Volume 13 Number 7
Journal of Advances in Physics

First principles calculations on the electronic and optical properties of zincblende $B_xGa_{1-x}As$, and $B_xIn_{1-x}As$ semiconductor alloys.

N.Amrane* and M. Benkraouda
Physics Department, U.A.E. University, Al-Ain, P.O. Box: 15551, U.A.E.
E-mail: namrane@uaeu.ac.ae

Abstract

A theoretical study of the electronic and optical properties of zincblende $B_xGa_{1-x}As$ and $B_xIn_{1-x}As$ semiconductor alloys is presented, using the full potential linearized augmented plane wave method. In this approach, the generalized gradient approximation was used for the exchange–correlation potential. Ground state properties such as lattice parameter and band structure are calculated as a function of the mole fraction.

We have also analyzed the optical properties (refractive index, dielectric function, real and imaginary), the 4x4 Kane's interaction matrix is calculated in order to ease simulations of optoelectronic devices. The results have been discussed in terms of previously existing experimental and theoretical data, and comparisons with similar compounds have been made.

Keywords

band structure, refractive index, reflectivity.

1-INTRODUCTION

With the advent of state-of-the-art techniques for growing semiconductor alloys on common substrates such as GaAs, silicon, and germanium, semiconductor compounds, which previously were very difficult to synthesize, are now routinely achieved. Techniques such as metal-organic chemical vapor deposition, molecular-beam epitaxy, and pulsed laser ablation have provided the opportunity to synthesize and study a large number of nitride, phosphide, and antimonide semiconductor alloys. Among the important group-III-V alloys with lattice match to GaAs, the III-V-boride compounds begin to attract interest [1-5]. The conduction band minimum is located along the Δ line at 0.8X [6]. The direct band gap is found to be in the 3.0–4.0 eV energy range by various semi-empirical or first-principles methods combined within the local density approximation (LDA) or the generalized gradient approximation (GGA) [7, 8]. Electronic excitation energies were calculated in the GW approximation to include the effects of exchange and correlation on the quasiparticle energies. It yields a direct band gap value of 4.0 eV and an indirect band gap value of 1.93 eV at the X point [9]. Despite many theoretical and experimental studies on binary boride materials, except for the BAs system for which physical material properties are largely obscure, only little is known for ternary and quaternary boron incorporating III-V solid solutions.

It recently appeared that the growth of the BxGa1−xAs alloy may be useful for obtaining the BGaInAs quaternary alloy or could be used as a tensile strained epilayer in the frame of strain compensation for InGaAsN−based heterostructures for emission at 1.3−1.5 mm. Despite this opportunity, little is known about the incorporation of boron into the group III sublattice which seems complex. Both the thermodynamical stability of the binary Bas compound and that of the alloy are questionable. A large gap of miscibility is also excepted as atomic boron is smaller than Ga. Demanding studies of fundamental properties, the incorporation of boron may open pathways for band-gap engineering in III-V alloys. Specifically, long-wavelength materials for solar cell absorber, coherent light emitter, and detector devices may enrich the realm of III-V optoelectronic applications.

Of particular recent interest are alloys of a wide gap semiconductor (e.g., nitrides) with a ''conventional'' Group-III–V semiconductor because of their promise in optical applications. Two diverging scenarios were considered: (i) using a significant amount ~10%–30% Of the wide gap component to shift the alloy band-gap to the blue (e.g., adding ~20% GaN to InN) for light-emitting diode or laser applications, and (ii) using a small amount of the wide gap semiconductor to shift the alloy band-gap to the red (e.g., adding 1%–3% GaN to GaAs) for photovoltaic applications. The latter effect occurs naturally if the band-gap bowing parameter b is larger than the difference of the band gaps of the constituents (e.g., ZnS-ZnTe; GaAs-GaN). In this case addition of small amounts of the wide gap components acts to initially lower the band gap of the small gap component. For example, one can achieve the technologically desired 1-eV gap if one adds nitrogen to GaAs or to InGaAs. When boron is substituted into GaAs, it can go to either a gallium site or an arsenic site. Normally boron prefers isovalent substitution on the gallium site, 1–3 which is the case we study here. In the other case when boron goes to the arsenic site ~a boron ''antisite'' defect, the boron acts as an acceptor and this antisite defect has been the subject of numerous studies [10–12] Growth conditions determine whether boron goes to the gallium site as an isovalent substitution or to the arsenic site as an acceptor. For example, BAs antisite defects.

2- CALCULATIONS

Scalar relativistic calculations have been performed using the wien2k code [13,14]. For the exchange correlation potential, we have used the local density approximation (LDA) with a parameterization of Ceperly-Adler data [15]. The new Full Potential Augmented Plane Wave method of the density functional theory is applied [16,17]. Several improvements to

DOI : 10.24297/jap.v13i7.6267
www.cirworld.com

solve the energy dependence of the basis set were tried but the first really successful one was the linearization scheme introduced by Andersen [18] leading to the linearized augmented plane wave (LAPW) method. In LAPW, the energy dependence of each radial wave function inside the atomic sphere is linearized by taking a linear combination of a solution u at a fixed linearization energy and its energy derivative $\dot{u}$ computed at the same energy.

$$\Phi_K(\mathbf{r}) = \begin{cases} \sum_L \left[a_L^{\alpha \mathbf{K}} u_l^{\alpha}(r') + b_L^{\alpha \mathbf{K}} \dot{u}_l^{\alpha}(r') \right] Y_L(\hat{r}') & r' \langle R_\alpha \\ \Omega^{-1/2} \exp\left(i(k+K).r\right) & r \in I \end{cases} \quad (1)$$

Where r'=r-r_α is the position inside sphere α with polar coordinates r' and r, **k** is a wave vector in the irreducible Brillouin zone, **K** is a reciprocal lattice vector and u_l^{α} is the numerical solution to the radial Schrodinger equation at the energy ε. The coefficients $a_L^{\alpha K}$ are chosen such that the atomic functions for all L components match (in value) the PW with K at the Muffin tin sphere boundary. The KS orbitals are expressed as a linear combinations of APWs $\Phi_K(r)$. In 1991 Singh [19] introduced the concept of local orbitals (LOs) which allow an efficient treatment of the semi-core states. An LO is constructed by the LAPW radial functions u and $\dot{u}$ at one energy ε_1 in the valence band region and a third radial function at ε_2.

$$\Phi_{LO}(\mathbf{r}) = \begin{cases} \left[a_L^{\alpha,LO} u_{1l}^{\alpha}(\mathbf{r}') + b_L^{\alpha,LO} \dot{u}_{1l}^{\varepsilon}(\mathbf{r}') + c_L^{\alpha,LO} u_{2l}^{\alpha}(\mathbf{r}') \right] Y_L(\hat{r}') & r' \langle R_\alpha \\ 0 & r \in I \end{cases} \quad (2)$$

Recently, an alternative approach was proposed by Sjöstedt et al [20], namely the APLW+ lo (local orbital) method. Here the augmentation is similar to the original APW scheme but each radial wavefunction is computed at a fixed linearization energy to avoid the non-linear eigenvalue problem. The missing variational freedom of the radial wavefunctions can be recovered by adding another type of local orbitals (termed in lower case to distinguish them from LO) containing u and $\dot{u}$ term:

$$\Phi_{lo}(\mathbf{r}) = \begin{cases} \left[a_L^{\alpha,lo} u_l^{\alpha}(\mathbf{r}') + b_L^{\alpha,lo} \dot{u}_l^{\alpha}(\mathbf{r}') \right] Y_L(\mathbf{r}') & r' \langle R_\alpha \\ 0 & r \in I \end{cases} \quad (3)$$

It was demonstrated that this new scheme converges faster than LAPW. The APW +lo scheme has been implemented in the wien2k code version [21].

However, in the calculations reported here, we chose the muffin tin radii for B, As, Ga and In to be 2.0, 1.9, 2.2 and 1.8 a.u. respectively. The expansion of the spherical region is developed up to l_{max}=10. Furthermore, we have used the energy cutoff of $R_{\square\square}.K_{\square\square\square}$=8 and the maximal reciprocal vector equal to 10. The integrals over the Brillouin zone are performed using the Monkorst-pack special k-points approach [22]. Since calculations of the optical properties require a moredense k-matrix, we have used 1000 k-points in the irreducible Brillouin zone for integration in reciprocal space.

Optical properties of a solid are usually described in terms of the complex dielectric function $\varepsilon(\omega) = \varepsilon_1(\omega) + i\varepsilon_2(\omega)$. The dielectric function is determined mainly by the transition between the valence and conduction bands according to perturbation theory, the imaginary part of the dielectric function in the long wavelength limit has been obtained directly from the electronic structure calculation, using the joint density of states (DOS) and the optical matrix elements. It is expressed as

$$\varepsilon_2(\omega) = \frac{4\pi^2 e^2}{3m^2\omega^2} \sum_{l,n} \int_{BZ} \frac{2}{(2\pi)^3} d^3k \left| P_{nl} \right|^2 .\delta\left[E_l(k) - E_n(k) - \hbar\omega \right] \quad (4)$$

Where m is the mass and e the electrical charge of the electron, $\sum_{l,n}$ means the summation between all the conduction bands (l) and valence bands (n); and P_{nl} expresses the momentum matrix element between l and n. It is given by

$$P_{nl} = \frac{m}{\hbar}\langle nk|\nabla_k H,(k)|lk\rangle$$

Where H(k) is the Hamiltonian, and $\langle nk|,|lk\rangle$ are the k-space wavefunctions. Using the FP-LAPW parameters, we can directly calculate P_{nl}.

The real part of the dielectric function can be derived from the imaginary part by the Kramers-Kronig relationship. The knowledge of both the real and the imaginary parts of the dielectric allows the calculation of important optical functions. In this paper, we also present and analyze the refractive index $n(\omega)$ given by

$$n(\omega) = \left[\frac{\varepsilon_1(\omega)}{2} + \frac{\sqrt{\varepsilon_1^2(\omega)+\varepsilon_2^2(\omega)}}{2}\right]^{1/2} \quad (5)$$

At low frequency (ω=0), we get the following relation:

$$n(0) = \varepsilon^{1/2}(0)$$

To correct the LDA error in the band gaps a constant potential was applied to the conduction band states (using the scissors operator which rigidly shifts the conduction band states) in order to match the calculated band gaps with the experimental data.

3. RESULTS

3.1 Electronic properties

In this section, we present LDA calculations on $B_xGa_{1-x}As$ and $B_xIn_{1-x}As$ alloys using the virtual crystal approximation (VCA). Fig. 1(a), (b), (c) and (d) represents the the electronic band structures along symmetry lines, The calculated band energy gaps at high symmetry points are given in table 1, the bandgaps of both alloys are found to be in close agreement with other theoretical calculations.

The variations of two direct band gaps and two indirect band gaps are presented as a function of the boron composition for $B_xGa_{1-x}As$ and $B_xIn_{1-x}As$. It must be pointed out that the various curves represent the Γ_{1c} _ Γ_{15v} and Γ_{1c} _ Γ_{15v} direct gaps and the Lc _ Γ_{15v} and Δc _ Γ_{15v} indirect gaps variations with respect to the top of the Γ_{15v} valence band.

ISSN 2347-3487
Volume 13 Number 7
Journal of Advances in Physics

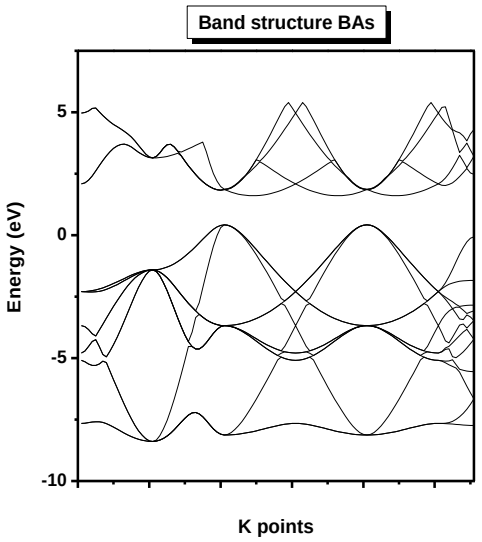

Figure 1(a): Band structure Bas

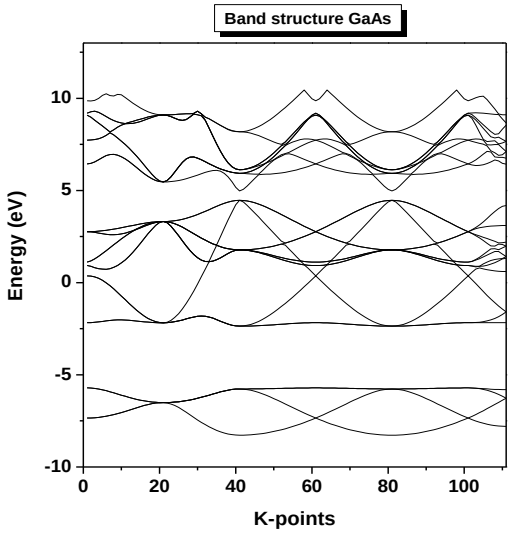

Figure 1(b): Band structure GaAs

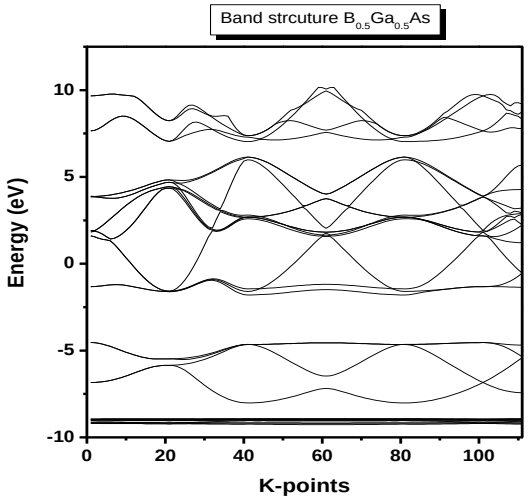

Figure 1(c): Band structure $B_{0.5}Ga_{0.5}As$

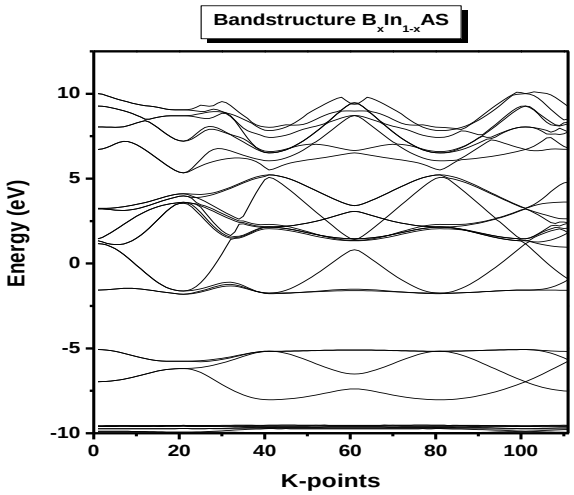

Figure 1(d): Band structure $B_{0.5}In_{0.5}As$

We may first consider the electronic properties of both pure compounds. For pure GaAs, the smallest band gap is the direct band Γ1c _ Γ15v. It is interesting to compare our calculated gaps with experimental data.

Table 1. Band energies (eV)

	Present work	**Other calculations**	**Experiment**
BAs	1.2 (GGA96)	1.8 eV (FP-LMTO)[a]	1.46[b]
GaAs	0.51(GGA96)	1.75(FP-LMTO)[a]	1.51[b]
InAs	-0.31(GGA96)	1.73(FP-LMTO)[a]	0.542[b]
$B_{0.5}Ga_{0.5}As$	0.3(GGA)	1.5 (FP-LMTO)[a]	0.93[b]
$B_{0.5}In_{0.5}As$	0.9	1.74(FP-LMTO)[a]	1.46[b]

[a] Reference [24]

[b] Reference [25]

Since quasi-particle excitations are not taken into account in density functional theory (DFT), the energy gap calculated from DFT, often called the Kohn-Sham gap, tends to be smaller than the experimental one. In some cases, even the wrong ground state is predicted, as, e.g., in Ge, where the energy gap is around 0.7 eV, whereas the LDA Kohn-Sham gap is slightly negative at ambient pressure [23]. The GGA corrections yield only minor improvement. Quasiparticle calculations essentially overcome the underestimate of the band gap as obtained using the LDA, and yield band structures in much better agreement with experiment; they are, however, time consuming and do not, as yet, produce self-consistent total-energy values. The GW calculations for GaN for instance also did not include the d states as valence states, but treated them as part of the pseudopotential core. However, Fig. 1(a) indicates that BAs with zinc blende structure has an indirect band gap between the top of the valence band and the bottom of the conduction band at the Γ point. The energy levels for the lower part of the valence band vary slowly and are attributed to the semi core-like B 3s states. The upper valence bands are mainly due to the As 2p orbitals and are much flatter as compared with the conduction bands, resulting in heavier effective masses for the valence band holes. This large disparity in the effective masses for the electron and the hole is one of the main reasons for the difficulty in fabricating BAs as highly conductive p-type materials.

3.2 Optical properties

The study of the optical constants and their variation with frequency is very interesting for the uses of films in optical applications. These applications require accurate knowledge of the optical constants over a wide wavelength range. Extinction coefficient and refractive index. The reflectivity (R) of materials of refractive index (n) and extinction coefficient (k) is given by:

$$R = \frac{(n-1)^2 + k}{(n+1)^2 - k} \tag{8}$$

An equation derived independently for the determination of the optical energy gap as:

$$\alpha(h\nu) = \frac{c}{h\nu}(h\nu - E_g)^m \tag{9}$$

Where m =1/2 for allowed direct transition, m =3/2 for direct ‘‘forbidden’’ transition, m =2 for allowed indirect transition and m =3 for indirect ‘‘forbidden’’ transition. C is a constant nearly independent on photon energy and known as the disorder parameter. Eg is closely related to energy band gap.

We now turn to the analysis of the optical spectra. The dielectric functions of $B_xGa_{1-x}As$ and $B_xIn_{1-x}As$ in the zinc blende structure are resolved into two components $\varepsilon_{xy}(\omega)$, average of the spectra for the polarization along the x and y-directions and ε_z, the polarization parallel to the z-direction. The calculated dielectric constants are shown in table 2.

Figure 2 (a), (b), (c) and (d) shows the variation of the imaginary part of the electronic dielectric function for $B_xGa_{1-x}As$ and $B_xIn_{1-x}As$, for radiation up to 12 eV. The calculated results are rigidly shifted upwards by 1.40 eV.

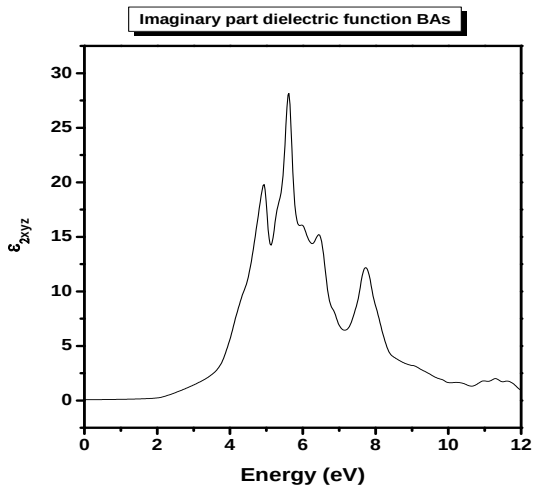

Figure 2(a): Imaginary part ε_2 BAs

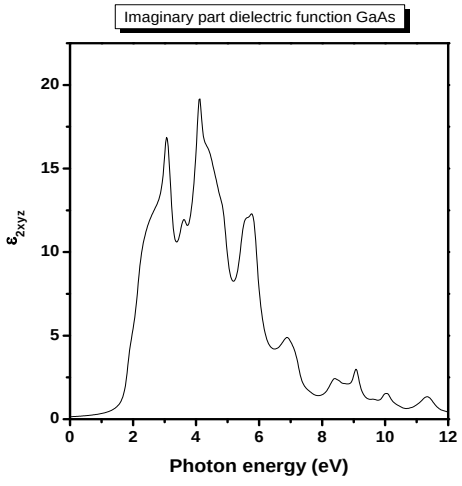

Figure 2(b) Imaginary part ε_2 GaAs

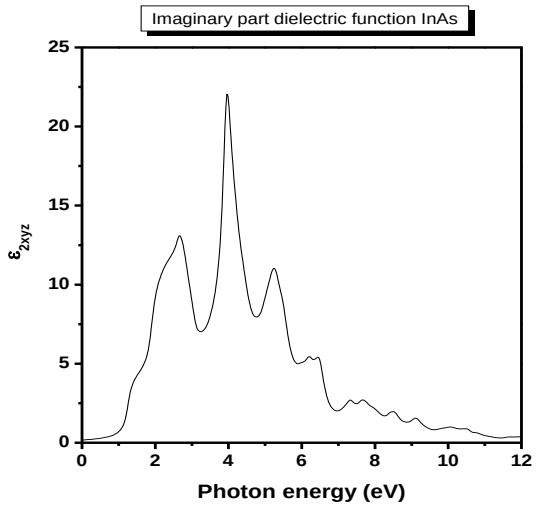

Figure 2(c): Imaginary part ε_2 InAs

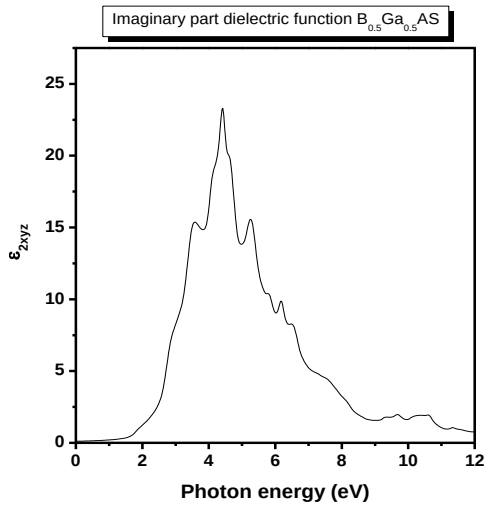

Figure 2(d): Imaginary part ε_2 $B_{0.5}Ga_{0.5}As$

The main feature is a broad peak with a maximum around 8 eV, 7.5 and 10 eV for BAs, GaAs and InAs respectively, and the maximum amplitude is at 4, 2 and 6.2; a shoulder is also visible at around 3.2 eV, 4, and 4.8 respectively. The peak as well as the shoulder are excellently reproduced in the calculations, as are the general form of some experimental spectra. There are also two other groups of peaks, in (11.2 eV- 14.3 eV) photon energy range, they are mainly due to transitions in the vicinity of M. this is usually associated with E_1 transition.

Next, we consider the dispersive part of the dielectric function, ε_1, see figure 3(a), (b), (c) and (d). The calculated spectra have been obtained by Kramers-Kronig transformation of the shifted ε_2 spectra. The main features are a shoulder at lower energies, a rather steep decrease for both alloys, between 3 and 8 eV, after which ε_1 becomes negative, a minimum and a slow increase toward zero at higher energies, the decrease is however more rapid as x increases in the $B_xGa_{1-x}As$ rather than the $B_xIn_{1-x}As$ alloy. The calculated dielectric constants compared with the experimental data and some other work are shown in table 2.

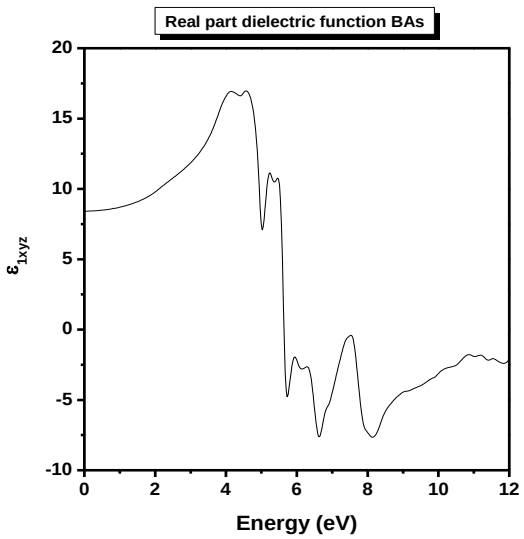

Figure 3(a): Real part ε_1 BAs

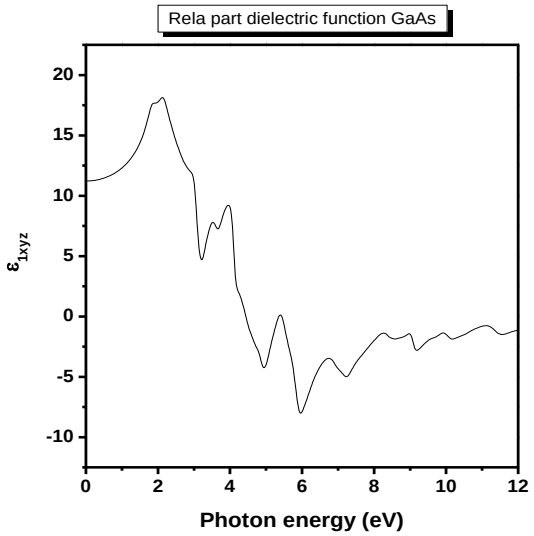

Figure 3(b): Real part ε_1 GaAs

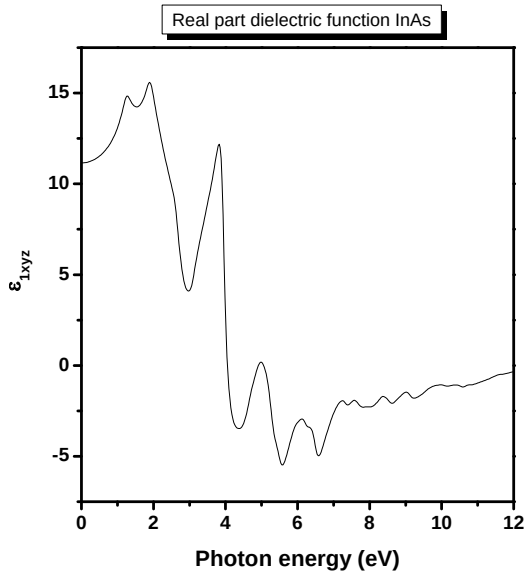

Figure 3(c): Real part ε_1 InAs

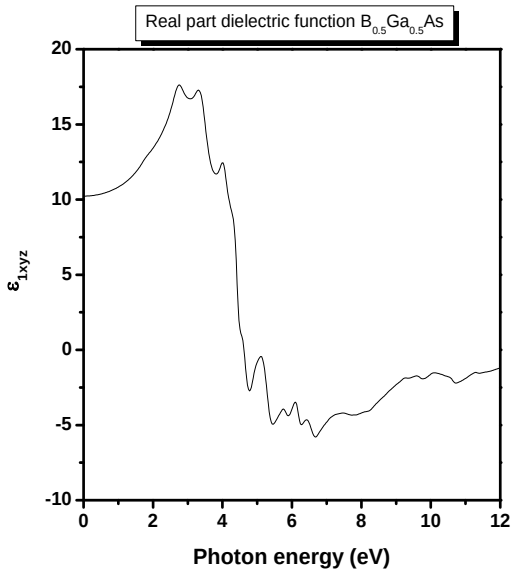

Figure 3(d): Real part ε_1

Table 2: The calculated dielectric constants

	Present work $\varepsilon_{\parallel}$	**Experiment** $\varepsilon_{\parallel}$
BAs	5.1	4.83[a]
GaAs	4.7	3.22[a]
InAs	3.2	2.9[a]
$B_{0.5}Ga_{0.5}As$	4.9	--
$B_{0.5}In_{0.5}As$	3.8	--

[a]reference [26]

We now shortly discuss the spectra obtainable from the dielectric function. As seen in figure 4 (which is not shown here), the refractive index was computed using both real and imaginary parts of the dielectric function. It shows that the refractive index exhibits a significant dispersion in the short wavelength region below λ= 290nm (3.15 eV) where absorption is strong. It decreases with the increase of the energy of the incident light, becoming nearly flat in the higher region. It is observed also that n reached a peak value at 2.55 eV and this peak occurred more or less at the same energy in the real part of the dielectric constant energy dependence curves.

We have fitted our calculated refractive index using the empirical formula of Peng and Piprek [27], given by the following relation:

$$n(E) = \left[a\left(\frac{E}{E_g}\right)^2 \left(2 - \left(1+\frac{E}{E_g}\right)^{0.5} - \left(1-\frac{E}{E_g}\right)^{0.5} \right) + b \right]^{0.5} \qquad (10)$$

Where the values of the direct energy gaps (E_g) are obtained from our optical spectra, and E is the photon energy.

CONCLUSION

The electronic and optical properties of $B_xGa_{1-x}As$ and $B_xIn_{1-x}As$ semiconductor alloys have been investigated using the wien2k package, full-potential linearized augmented plane wave (FP-LAPW) approach within the density functional theory (DFT) in the local spin density approximation (LSDA) including the generalized gradient approximation (GGA) was used. The use of GGA for the exchange-correlation potential permitted us to obtain good structural parameters. The calculated band-gap was also in good agreement with the other theoretical calculations. The real and imaginary parts of the dielectric functions were calculated for polarization in the x,y plane and along the z-axis, the optical properties are excellently reproduced using the density functional theory, if we allow for a rigid shift of the band structure , the so-called scissors operator.

REFERENCES

[1] Gus L. W. Hart, Alex Zunger, Phys. Rev. B 62, 13522 (2000)

[2] T. Hofmann, M. Schubert, G. Leibiger, V. Gottschalch, App. Phys. Let. 90, 182110 (2007)

[3] Shaoqing WANG, Journal of the Physical Society of Japan Vol. 78, No. 2, February, 2009

[4] A. Zaoui, F. El Haj Hassan, J. Phys.: Condens. Matter 13 (2001) 253.

[5] N.G. Szwacki, P. Bogulawski, Phys. Rev. B 64 (2001) 161201.

[6] N. Chimot, J. Even, H. Folliot, S. Loualiche, Physica B 364 (2005) 263–272

[7] G.L.W. Hart, A. Zunger, Phys. Rev. B 62 (2000) 13522.

[8] A. Zaoui, F. El Haj Hassan, J. Phys.: Condens. Matter 13 (2001) 253.

[9] M.P. Surh, S.G. Louie, M.L. Cohen, Phys. Rev. B 43 (1991) 9126.

[10] G. Zollo and R. M. Nieminen, J. Phys.: Condens. Matter, vol. 15, pp. 843–853, 2003.

[11] O. P¨atzold, G. G¨artner, and G. Irmer, phys. stat. sol. (b), vol. 232, pp. 314–322, 2002.

[12] N. Chimot et al. Physica B 364 (2005) 263–272

[13] K. Schwarz, P. Blaha, G.K.H.Madsen, Computer Physics Communications 147 (2002) 71–76

[14] J. A. Camargo-Martínez, R. Baquero, Revista Mexicana de F'isica 59, 453 (2013)

[15] D.M.Ceperley, B.I.Alder, Phys.Rev.Lett.45 (1990) 566

[16] A Zaoui and F El Haj Hassan, J. Phys.: Condens. Matter 13 (2001) 253–262

[17] Gulans A, Kontur S, Meisenbichler C, Nabok D, Pavone P, Rigamonti S, Sagmeister S, Werner U, Draxl C., J Phys Condens Matter. 26(36):363202. (2014)

[18] O.K.Andersen, Phys.Rev.B12 (1975) 3060-3083

[19] D.Singh, Phys.Rev.B 43 (1991) 6388-6392

[20] E.Sjöstedt, L.Nordström, D.J.Singh, Solid State Comm.114 (2000) 15-20

[21] K.Schwarz, P.Blaha, Comput.Mater.Sci. 28 (2003) 259

[22] H.J.Monkhorst, J.D.Pack, Phys.Rev.B13 (1976) 5188.

[23] M.Alouani and J.M.Wills, Phys.Rev.B54, 2480 (1996).

[24] N.Chimot et al. Physica B 364 (2005) 263–272.

[25] T. Hofmann et al. Appl. Phys. Let. 90, 182110 (2007).

[26] A. Zaoui, A.Yagoubi , Physica B.Vol 367,!93-204, (2005).

[27] T.Peng and J.Piprek, Electron. Let. 32, 24 (1996).

DOI : 10.24297/jap.v13i7.6267